PAPER

Soliton signature in the phonon spectrum of twisted bilayer graphene

IOP Publishing 2D Mater. 7 (2020) 025050 https://doi.org/10.1088/2053-1583/ab7874

2D Materials

PAPER

RECEIVED
21 January 2020

REVISED
16 February 2020

ACCEPTED FOR PUBLICATION
20 February 2020

PUBLISHED
19 March 2020

Soliton signature in the phonon spectrum of twisted bilayer graphene

Michael Lamparski, Benoit Van Troeye and Vincent Meunier

Department of Physics, Applied Physics, and Astronomy, Rensselaer Polytechnic Institute, Troy, New York 12180, United States of America

E-mail: MEUNIV@rpi.edu

Keywords: bilayer graphene, phonon band structure, solitons

Abstract

The phonon spectra of twisted bilayer graphene (tBLG) are analyzed for a series of 692 twisting angle values in the $[0, 30°]$ range. The evolution of the phonon bandstructure as a function of twist angle is examined using a band unfolding scheme where the large number of phonon modes computed at the Γ point for the large moiré tBLG supercells are unfolded onto the Brillouin Zone (BZ) of one of the two constituent layers. In addition to changes to the low-frequency breathing and shear modes, a series of well-defined side-bands around high-symmetry points of the extended BZ emerge due to the twist angle-dependent structural relaxation. The results are rationalized by introducing a nearly-free-phonon model that highlights the central role played by solitons in the description of the new phonon branches, which are particularly pronounced for structures with small twist angles, below a buckling angle of $\theta_B \sim 3.75°$.

Unconventional superconductivity and magnetism were not typically associated with graphene until very recently with the observation of strong electronic correlation in bilayer graphene twisted roughly at the $\theta = 1.1°$ *magic* angle [1–5]. This effect is related to the emergence of flat electronic bands with narrow band width [1, 5–9], and theoretical studies have established the importance of structural relaxation in the description of these phenomena [6, 8–18]. The atomic relaxation in twisted bilayer graphene (tBLG) is linked to the development of strain fields that tend to minimize the unfavorable AA-stacking regions—with local buckling—and lead to the formation of triangular domain patterns in the moiré pattern. This structural re-arrangement can be interpreted as the formation of solitons in the system [10, 19, 20].

Most of the existing theoretical studies devoted to tBLGs have focused on electronic properties. However, tBLG phonons are also expected to be affected by the formation of the moiré superlattice and its underlying strain fields, since they fundamentally correspond to excitations of the lattice [14, 21, 22]. Studying the large unit-cells corresponding to small values of twisting angles is computationally challenging and a fine analysis of the tBLG phonons has proven difficult, since a full treatment requires the calculations of dynamical matrices of with tens of thousand elements for structures prepared at a minimum energy configuration. Angeli and co-workers [22] were able to identify 10 nearly-flat energy phonon bands—not present in single- or bi-layer (Bernal) graphene—among the ∼30 000 phonon modes of one specific tBLG. At the same time, continuum models have predicted band gap openings at the zone border of the tBLG reciprocal lattices [15, 23, 24]. These studies are promising but need additional refinements to include buckling. Previous studies have investigated the Raman profiles of the G and 2D peaks of tBLGs, both theoretically and experimentally [25, 26]. These studies however did not consider any change in terms of phonon band structures theoretically but rather focused on peak intensity in resonance.

In this Letter, we overcome the technical difficulty of analyzing the large number of phonon modes of tBLG by adopting an unfolding scheme [27]. The many phonon modes of the superlattice are unfolded onto the reciprocal lattice of the bottom layer of graphene. This allows us to demonstrate the existence of a rich phononic structure, especially for small twist angles. The present study not only confirms the emergence of new phonon side-bands at the high-symmetry points of the graphene reciprocal lattice, but it also predicts a number of features that are specific to tBLGs. In particular, our study predicts very significant band splitting as large as 50 cm^{-1} for the high-frequency *G* modes at the zone center

of structures with small twist angles. A careful monitoring of the high-symmetry phonon modes as a function of the twist angle reveals the elaborate, but continuous, evolution of these phonon side-bands for $\theta \to 0$. Notably, the layer breathing mode at the zone center splits into several bands for decreasing angle—some showing evanescent character, others featuring mixed in-plane and out-of-plane characters.

A large number of tBLG superlattices are constructed following a procedure similar to the one presented in reference [28]. Certain discrete twist angles produce a commensuration between the layers, described by the equation $\mathbf{C}_B\mathbf{B} = \mathbf{L} = \mathbf{C}_T\mathbf{T}$, where $\mathbf{B}$ and $\mathbf{T}$ are matrices whose rows are basis vectors for each layer's lattice (bottom and top), $\mathbf{L}$ is the same for the commensuration cell, and $\mathbf{C}_B$ and $\mathbf{C}_T$ are integer matrices. Beginning from this premise and applying a series of number theoretical arguments, a one-to-one correspondence can be found between twist angles $\theta \in [0°, 60°]$ and coprime integer pairs (p, q) with $0 \leq p \leq q$. These solutions have twist angles and numbers of graphene unit cell per layer defined by [28]

$$\cos\theta = \frac{3q^2 - p^2}{3q^2 + p^2}, \tag{1}$$

$$N = \frac{3}{\delta}\frac{1}{\gamma^2}(3q^2 + p^2) = \frac{3q^2 + p^2}{(\frac{2}{\gcd(pq,2)})^2 \gcd(p,3)}, \tag{2}$$

where $\delta = 3/\gcd(p, 3)$ and $\gamma = 2\gcd(p, 3)/\gcd(pq, 2)$ are small positive integers, while gcd stands the greatest common divisor function. $N_C = 4$ N corresponds the number of carbon atoms in the graphene unit cell. There are in principle an infinitude of twist angles that lead to a commensurate structure, but only 692 of these angles in the range $0° \leq \theta \leq 30°$ produce a structure containing fewer than 20 000 atoms. Those are the systems we investigate in this work.

We use classical force-fields for structural relaxation and to compute the corresponding phonons in the harmonic approximation. Intralayer forces are computed using the second-generation REBO potential [29], while interlayer forces are modeled using the registry-dependent Kolmogorov–Crespi (KC) potential [30], in its local normal formulation. All atomic positions and lattice parameters of the superlattice are optimized with a conjugate gradient (CG) algorithm. The latter are found to vary in a negligible manner compared to the rigidly-stacked case. After CG convergence of all force components within 10^{-3} eV/atom, the dynamical matrix at Γ is computed using finite differences and then diagonalized. The presence of many local extrema makes the accurate relaxation of tBLG tedious. However, we take advantage of the phonon calculation to operate an iterative assessment of dynamical stability. In practice, when modes are found with negative eigenvalues (and if they are not translational acoustic modes), CG is performed again in a reduced parameter space where each parameter corresponds to one of the negative modes. This accelerated procedure can in theory be repeated until all negative modes are removed from the system. Unfortunately, suppressing the entirety of the negative modes for the small twist angle structures has been found to be particularly challenging (> 11 iterations required); however, the imaginary frequencies of these modes have a magnitude $< 4\ \mathrm{cm}^{-1}$ and are thus assumed to have negligible influence on the oncoming discussion.

Similar to previous studies [6, 10–16], accommodation between the layers is observed in order to minimize the AA-stacking region, which proves especially significant for small twist angles. Buckling is found to occur for certain structures with twist angles that are below some critical *buckling angle* θ_B, defined here as the angle below which negative modes are observed for the corresponding structure after one full CG relaxation. This definition accounts for the fact these non-zero modes are responsible for the buckling of the system. Here, we find $\theta_B \sim 3.75°$, meaning that all structures below this angle buckle, with the notable exception of a few structures (e.g. 3.482° and 3.150°, with $(p, q) = (1, 19)$ and $(p, q) = (1, 21)$, respectively) that have particularly small unit cells. The variation of the interlayer distance can be quite significant for small misalignment angles, i.e. as large as ∼0.23 Å for the 1.085° structure (see figure 1(d)). The magnitude of this variation is comparable to previous studies with classical potentials [11, 17, 18] and DFT computations [9].

As a reference, figure 1(a) represents the phonon band structure of Bernal-stacked bilayer graphene as computed with the REBO+KC potential. This potential has difficulty describing the dispersion of the high-frequency branch [31], but all of the other branches of graphene are qualitatively reproduced. Note that it also appears to somewhat underestimate the strength of the interlayer interactions: the shear mode for AB-stacked graphene is found to be 19.7 cm^{-1} (versus 32 cm^{-1} from experiment [32]), and the layer-breathing mode in structures around 12° is found to be ∼79 cm^{-1} (versus ∼95 cm^{-1} from experiment [33]).

Analyzing the effect of twist angle on the phonon modes in tBLGs is particularly difficult since each structure has a very large number (3 N) of normal modes, and this number varies among all structures considered. To address this issue, the phonon data calculated at the supercell zone center Γ_L (i.e. Γ in the small BZ of the tBLG) are unfolded onto the BZ of reciprocal cell of the primitive cell of one of the layers, producing a band structure in the single-layer first Brillouin zone (FBZ) [27]. This process is *fuzzy* in the sense that a mode in the supercell is usually expressed a linear combination of single-layer modes with different wavevectors. Note also

that the images of Γ_L in the reciprocal cell of one layer are not compatible with the translational symmetry of the other layer; thus, the unfolding process exclusively considers the projections of the normal modes onto a single layer. Applying the unfolding method requires the construction of translation operators $\hat{T}(R)$ for R in the quotient group $\mathbf{L}_B/\mathbf{L}_L$, where $\mathbf{L}_B$ is the real-space lattice of the bottom layer, and $\mathbf{L}_L$ is the moiré lattice. Ideally, we apply these operators to a Bloch function represented in the form of a 3 N-dimensional vector $\mathbf{u_K}$ (for some $\mathbf{K}$ in the moiré FBZ), containing Cartesian components at each site in the moiré cell.

Prior to relaxation, it can be seen that each translation operator may take the form $\hat{T}(R)\,\mathbf{u_K} = \mathbf{Q_{K,R}P_R u_K}$, where $\mathbf{P_R}$ is a permutation matrix (obtained by recognizing that the translation is a symmetry of the atomic coordinates in this layer), and $\mathbf{Q_{K,R}}$ is a diagonal matrix of corrective phase factors (fixing the Bloch phases for atoms that are translated between different images of the moiré cell). Strictly speaking, after relaxation, these quotient group translations are no longer symmetries of the atomic coordinates within the layer. However, we may continue to use the above result by taking as an approximation that the atoms vibrate around their unrelaxed positions for the purpose of unfolding. This assumption is violated somewhat in small angle structures, especially due to out-of-plane buckling. However, this out-of-plane motion is not expected to meaningfully affect the unfolding probabilities onto points that lie in the plane.

We find that even at a moderately-sized angle of 9.737° (not shown here), the unfolded band structure exhibits no features significantly different from those of Bernal stacking, except for the shear mode frequency (which is much lower than that of Bernal bilayer graphene due to a reduced effective interlayer force constant). In stark contrast, at small nonzero twist angles, several additional prominent features appear in the unfolded bands. For instance, figure 1(e) depicts the unfolded representation for the phonons of the 1.085° ($(p, q) = (1, 61)$) twist-angle structure. This phonon band structure exhibits the basic features of the AB-stacked bilayer graphene, including the prominent splitting of the out-of-plane acoustic (ZA) band to produce a layer-breathing mode. In addition, there is splitting of the G band at the single-layer Γ, by about 60 cm^{-1} at $\theta = 1.085°$. In addition to this splitting, branches form in a number of side-bands around the single-layer M and K points. Structural relaxation plays a critical role in all of these effects; for comparison, band plots are included for structures with and without relaxation in figures 1(e) and (b), respectively. A plot of the in-plane displacement fields minimizing the AA-stacking region is shown in figure 1(c), while the variation of the interlayer distance is provided in figure 1(d) to highlight the buckling in the vicinity of the AA-stacking region. Clearly, without relaxation, none of the side band effects are apparent, and the phonon band structure is extremely similar to the case of Bernal graphene bilayer, except for a reduced shear mode frequency. In contrast to what previous theoretical works predict [23, 24], we do not find any particularly pronounced renormalization of the speed velocity in twisted bilayer graphene.

The plots in figure 2 focus on specific high-symmetry points in the single-layer Brillouin Zone and compare the unfolded bands between different structures. Figure 2 (a) shows the evolution of the bands at M_B with respect to changing angle. In this plot, only data from Γ_L point is used. M_B is not an image of Γ_L under the moiré reciprocal lattice; thus, for each structure, the data at the nearest image of Γ_L is used. For many of these structures (particularly those with smaller commensurate cells), this image may be far away from M_B, resulting in poor-quality data; therefore, we omit structures where the nearest image of Γ_L is further than $0.01 \times 2\pi\mathrm{\AA}^{-1}$ from M_B. The in-plane transverse acoustic (TA) and longitudinal acoustic (LA) bands can be observed to split into increasingly many side bands as angle decreases (though there is no splitting at 0°).

Unfolded probability data at Γ_B are available for all 692 structures, and are shown in figures 2(b) and (c). Astonishingly, all the modes do not undergo a continuous transformation from 30° to 0°. Perhaps most strikingly is what happens to the layer breathing mode (figure 2(b) around 80 cm^{-1}), which is well defined at large angles but splits into several branches for decreasing angles. One of them shows a linear dependency that can be extrapolated onto the shear mode at 0°, implying that this mode shows both in-plane and out-of-plane characters for small twist angles. The others are evanescent and show complex behavior as a function of twist angle. Nevertheless, their general trend seems to follow the expectation value of the dynamical matrix for the layer breathing mode in the system (i.e. matrix element of the dynamical matrix for a pure breathing mode; red curve in figure 2(b)), and appears to eventually converge to the value of the layer breathing mode in Bernal graphene bilayer for $\theta \to 0°$.

Finally, the high-frequency modes at the tBLG zone center are represented in figure 2(c). Similar to the modes shown in figure 2(a), more and more side bands emerge for decreasing angles. Notably, there are several branches that take values higher than that of the G mode computed in Bernal graphene bilayer. It should be emphasized that this is the most striking signature of twisting angle and it could, in principle, be used as a fingerprint of a specific twisting angle.

We will now discuss the fundamental origin of the tBLG-specific phonon side bands, starting from the Frenkel-Kontorova (FK) model [19, 35]. This classical model considers a 1D chain of atoms placed into a periodic external potential whose period differs

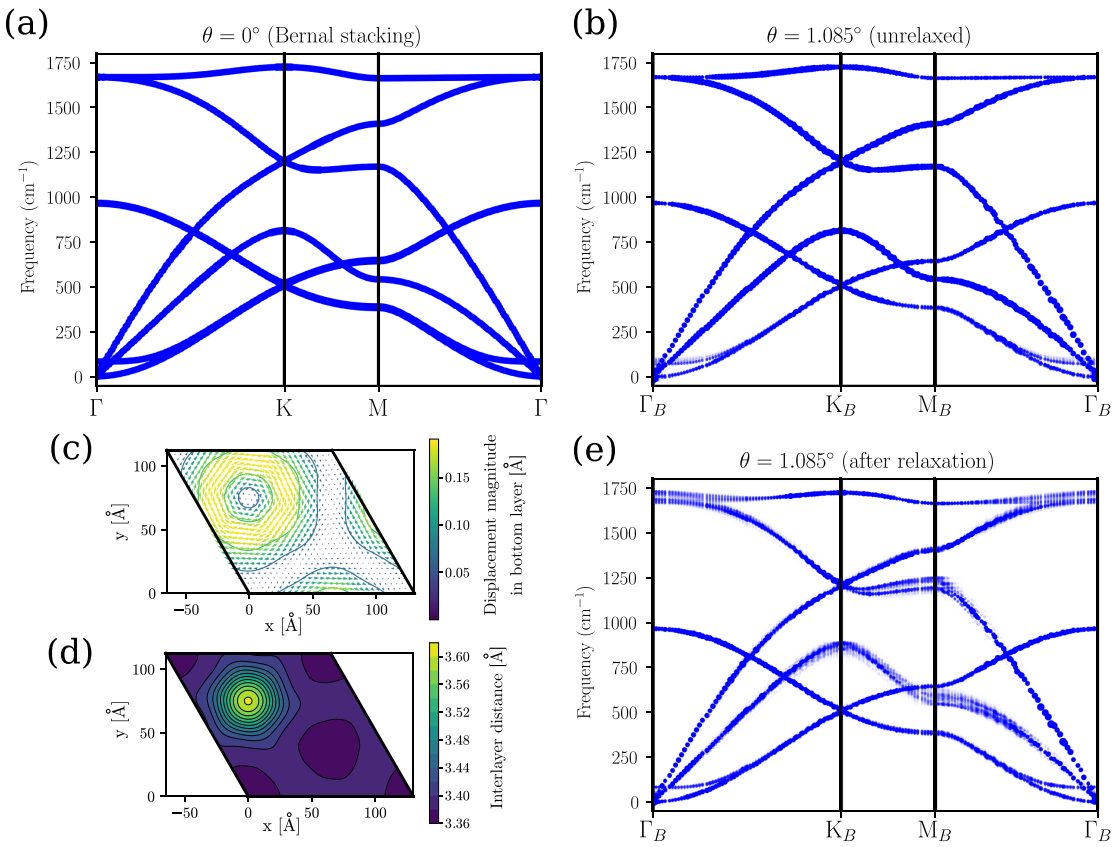

Figure 1. (a) Phonon band structure of graphene bilayer in the Bernal stacking configuration. (b) Unfolded phonon band structure of twisted bilayer graphene structure with rotation angle 1.085° prior to relaxation. The *B* subscripts denote that the high symmetry path is taken along the Brillouin zone of the bottom layer, and each position on the x-axis displays data unfolded onto the nearest point that is an image of Γ_L, M_L, or K_L. (c) In-plane displacement field in the bottom layer of the 1.085° twist-angle structure. Close to the AA-stacking region, this layer tends to rotate clockwise in order to minimize the region of AA stacking. (d) Variation of the interlayer distance for the 1.085° twist-angle structure. The most pronounced variations are observed close the AA-stacking region, indicating local buckling of the layers. (e) Unfolded phonon band structure of the 1.085° twist-angle structure after relaxation. Compared to the unrelaxed case (panel (c)), significant splitting can be seen at M, K, and in the G band.

from the one of the chain. In general, its ground state consists of the periodic repetition of solitons that separate regions where the atoms sit in the close neighborhood of potential minima [19]. Those solitons can be interpreted as new quasi-particles of the system, and they behave relativistically since their dynamics are dictated by the Sine-Gordon equation [34]. Note that in addition to a soliton solution, the formal problem admits another type of quasi-particle solution called *breathers*. These consist of non-linear waves oscillating in time but localized in space [34].

Investigating the dynamics of breathers and solitons is a problem of interest on its own. However, we shall here focus on examining how their static configuration affect the phonons. The soliton network deforms the lattice periodically, generating a potential that is felt by the otherwise-free (i.e. independent) phonons. While the analytical expression of this potential can be exactly derived within the FK model, we will simply write it here in terms of its Fourier series for sake of simplicity:

$$V_{sol}(x_n) = \sum_t \tilde{V}_t e^{itQx_n}, \quad (3)$$

where x_n is the position of the n*th* atom of the 1D chain, $\tilde{V}_t$ are the Fourier components of the decomposition and Q is the superlattice wave vector. The $\tilde{V}_t$ coefficients are thus taken here as parameters. This soliton potential acts on the motion of phonons as follows:

$$m\omega^2\overline{u}_n = \lambda(2\overline{u}_n - \overline{u}_{n-1} - \overline{u}_{n+1}) + V_{sol}(x_n)\overline{u}_n, \quad (4)$$

where m is the mass of the atoms of the chain, ω is the phonon frequency, $\overline{u}_n$ the atomic displacement and λ the spring constant of the chain. The first term of the right-hand side of the equation is nothing more than the force felt by the atom n in the isolated 1D chain. Let us suppose now that this soliton potential is weak and thus can be treated perturbatively. Then, one can solve equation (4) using perturbation theory. This problem strongly resembles the one described by the nearly-free electron (NFE) model [35], except that the electrons and the ionic potential are replaced by the phonons and the soliton potential, respectively. Insights into the phonons under the soliton potential, hereby referred to as the NFP model, can therefore be extracted from the nearly-free electron (NFE) model.

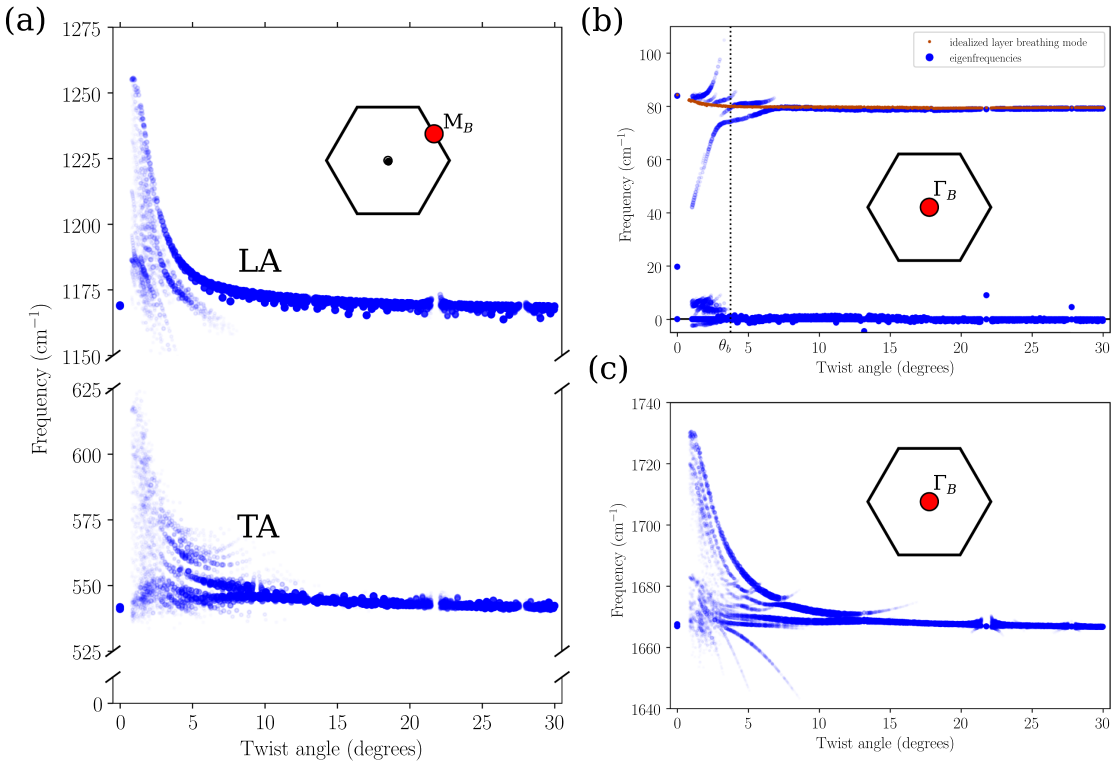

Figure 2. (a) Phonon bands unfolded from the moiré Γ point onto the single-layer M point at a variety of twist angles. Of the 692 tBLG structures with under 20000 atoms per cell, only 617 of them have an image of Γ_L that lies within $0.01 \times 2\pi\text{Å}^{-1}$ from M_B; the rest are not shown (except for the data at 0°, which is computed without unfolding). (b)-(c) Phonon bands unfolded onto the single-layer Γ point for all 692 structures at (b) low and (c) high frequencies (i.e. including graphene's G band). The low frequency plot includes the frequencies derived from the expectation value of a pure layer-breathing mode (red). The lower frequency values correspond to shear-like modes. Structures below $\theta_B = 3.75°$ are found after CG to have buckling modes that produce more energetically favorable structures. Relaxation is performed along these modes up to three times.

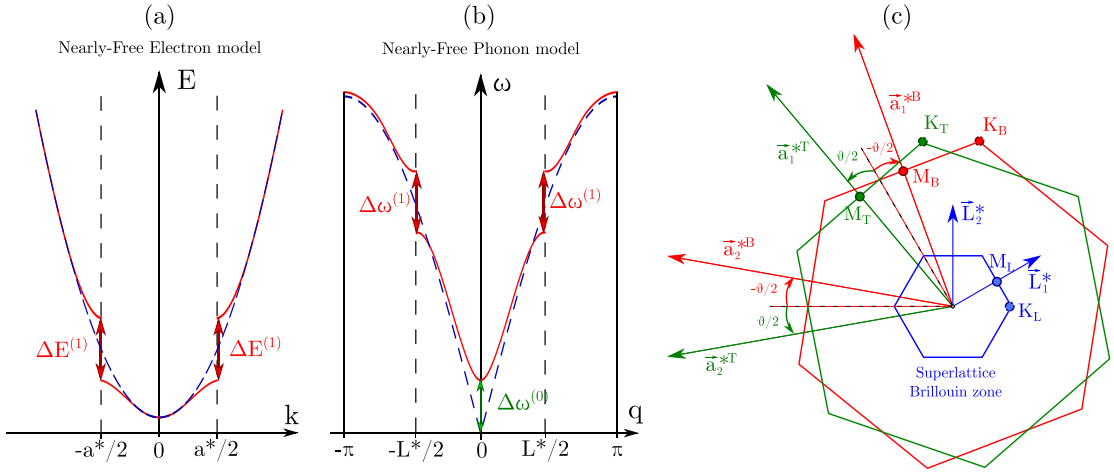

Figure 3. (a)-(b) Schematic representation of the predictions of the NFE and nearly-free phonon (NFP) models, truncated to the first potential harmonic for the sake of legibility. The dashed blue lines represent the unperturbed spectra, i.e. the free electrons and free phonons, while the red lines correspond to the perturbed solutions. Both models predict a band gap opening either at the lattice Brillouin zone $a^*/2$ (NFE model) or at the superlattice Brillouin zone $L^*/2$ (NFP model). In addition, the NFP model leads to the transformation of the acoustic phonon into an optical one. (Right) Schematic representation of the Brillouin zones of the rotated graphene lattice and of the superlattice. Due to the geometry of the problem, a high-symmetry point lying on the superlattice Brillouin zone corresponds exactly to the difference in terms of position between the corresponding high-symmetry points in the bottom and top layers (e.g. M_L, M_B and M_T).

The NFE model accounts for the opening of band gaps in the electronic band structure, located at the zone borders for the odd harmonics of the ionic potential and at the zone center for the even harmonics (see figure 3(a)). The mean value of the potential is generally discarded since it simply leads to a rigid energy shift. Restricting the analysis to the first harmonic of the potential, the band gap opening

at zone borders is associated with the formation of stationary waves: the electrons are either localized around the nuclei (lower energy state) or away from them (upper energy state).

The results for phonons in the NFP model are unsurprisingly similar to the ones derived in the NFE model for electrons with the emergence of band gaps associated with stationary waves involving the displacement (or pinning) of the soliton cores. The theoretical details will be detailed elsewhere but the main results are shown in figure 3(b). A number of differences with respect to the NFE model should be noted. First, the spectra of free electrons and free phonons differ: the former is unbound ($E \propto k^2$, where E is the energy and k the electron wavenumber) while the latter is bound ($\omega^2 \propto \sin^2(q/2)$, where ω is the frequency and q the phonon wavenumber). This translates into noticeable differences in the dispersion relations of the two nearly-free models. Second and more fundamentally, the acoustic mode present in the isolated 1D chain is transformed into an optical mode in the NFP model ($\Delta\omega^{(0)}$ opening in figure 3). This comes from the fact that the mean value of the potential cannot be discarded in the case of phonons since the soliton perturbation is acting over the square of the frequency (see equation (4)). This contrasts with the NFE model, where the perturbation acts directly on the energy and could therefore be disposed of.

The emergence of phonon side bands instead of band gaps as predicted by the NFP model is a particularity of the twisted bilayer system. To understand this, it is useful to inspect the BZ of the constituent layers with respect to that of the superlattice (see figure 3(c)). By geometrical construction, the superlattice reciprocal vectors correspond exactly to the difference between the reciprocal vectors of the bottom and top layers [6, 23]. As a consequence, the phonons at the M_L superlattice high-symmetry points correspond to phonon states at the M_B and M_T high-symmetry points in the bottom and top layers, respectively. The same reasoning holds for the K_L high-symmetry point. As discussed before, the NFP model indicates that a band gap is expected to open at the high-symmetry points of the superlattice Brillouin zone. It follows that the first soliton potential harmonic opens a band gap at the M_L point with amplitude $\Delta\omega^{(1)}$ and the third harmonic opens a band gap of amplitude $\Delta\omega^{(3)}$ at the same point, etc The mechanism hinges on the fact that, in contrast to electronic potential, the dispersion relation of phonon is bound: the band gap openings always affect the same initial phonon state, leading to the creation of different phonon side bands around the same frequency window. This explains the origin of the numerous phonon side bands presented in figure 1, which can thus be understood as the intrinsic signature of solitons in the system.

To summarize, we find the rich phononic structure for small twist angles in tBLGs is closely associated with the formation of a soliton network and can be explained in terms of the NFP model introduced here. Fundamentally, compared to the NFE model, the role of electrons and nuclear potential are fulfilled by the phonons and soliton potentials in the NFP model, respectively. The general framework allows us to contrast the results of the NFP and NFE models, in term of the different dispersion relations adopted by the phonons and electrons.

One should mention that, while we chose the single-layer FBZ as a support for unfolding, the mechanism of band unfolding is not unique and can be applied to other choices of BZ. For this reason, a number of bands cannot be directly seen in plots such as those presented in figure 1. For example, the R bands described by Jorio *et al* in reference [36] do not lie along the high symmetry path chosen here but can be obtained in a way similar to the procedure described in this Letter. This effect is outside of the scope of the present study and will be discussed in details elsewhere.

Acknowledgments

This work is supported by the NY State Empire State Development's Division of Science, Technology and Innovation (NYSTAR) through Focus Center-NY–RPI Contract C150117.

ORCID iDs

Benoit Van Troeye https://orcid.org/0000-0003-2073-1188
Vincent Meunier https://orcid.org/0000-0002-7013-179X

References

[1] Cao Y, Fatemi V, Fang S, Watanabe K, Taniguchi T, Kaxiras E and Jarillo-Herrero P 2018 *Nature* **556** 43
[2] Cao Y *et al* 2018 *Nature* **556** 80
[3] Yankowitz M, Chen S, Polshyn H, Zhang Y, Watanabe K, Taniguchi T, Graf D, Young A F and Dean C R 2019 *Science* **363** 1059
[4] Sharpe A L, Fox E J, Barnard A W, Finney J, Watanabe K, Taniguchi T, Kastner M A and Goldhaber-Gordon D 2019 *Science* **365** 605
[5] Codecido E *et al* 2019 *Sci. Adv.* **5** eaaw9770
[6] Nam N N T and Koshino M 2017 *Phys. Rev.* B **96** 075311
[7] Uchida K, Furuya S, Iwata J I and Oshiyama A 2014 *Phys. Rev.* B **90** 155451
[8] Guinea F and Walet N R 2019 *Phys. Rev.* B **99** 205134
[9] Lucignano P, Alfè D, Cataudella V, Ninno D and Cantele G 2019 *Phys. Rev.* B **99** 195419
[10] Alden J S, Tsen A W, Huang P Y, Hovden R, Brown L, Park J, Muller D A and McEuen P L 2013 *Proc. of the National Academy of Sciences* textbf110 p 11256
[11] van Wijk M M, Schuring A, Katsnelson M I and Fasolino A 2015 *2D Materials* **2** 034010
[12] Dai S, Xiang Y and Srolovitz D J 2016 *Nano Lett.* **16** 5923
[13] Jain S K, Juričić V and Barkema G T 2016 *2D Materials* **4** 015018
[14] Choi Y W and Choi H J 2018 *Phys. Rev.* B **98** 241412
[15] Koshino M and Nam N N T 2019 arXiv: 1909.10786

[16] Yoo H et al 2019 Nat. Mater. 18 448
[17] Gargiulo F and Yazyev O V 2017 2D Materials 5 015019
[18] Angeli M, Mandelli D, Valli A, Amaricci A, Capone M, Tosatti E and Fabrizio M 2018 Phys. Rev. B 98 235137
[19] Frank F C and van der Merwe J H 1949 Proc. Royal Soc. Lond. 198 p 205
[20] Popov A M, Lebedeva I V, Knizhnik A A, Lozovik Y E and Potapkin B V 2011 Phys. Rev. B 84 045404
[21] Cocemasov A I, Nika D L and Balandin A A 2013 Phys. Rev. B 88 035428
[22] Angeli M, Tosatti E and Fabrizio M 2019 Phys. Rev. B 9 041010
[23] Koshino M and Son Y-W 2019 Phys. Rev. B 100 075416
[24] Ochoa H 2019 Phys. Rev. B 100 155426
[25] Kim K et al 2012 Phys. Rev. Lett. 108 246103
[26] Coh S, Tan L Z, Louie S G and Cohen M L 2013 Phys. Rev. B 88 165431
[27] Allen P B Berlijn T Casavant D A and Soler J M 2013 Phys. Rev. B 87 085322
[28] Shallcross S, Sharma S, Kandelaki E and Pankratov O A 2010 Phys. Rev. B 81 165105
[29] Brenner D W, Shenderova O A, Harrison J A, Stuart S J, Ni B and Sinnott S B 2002 J. Phys.: Condens. Matter. 14 783
[30] Kolmogorov A N and Crespi V H 2005 Phys. Rev. B 71 235415
[31] Maultzsch J, Reich S, Thomsen C, Requardt H and Ordejón P 2004 Phys. Rev. Lett. 92 075501
[32] Tan P H et al 2012 Nat. Mater. 11 294
[33] He R et al 2013 Nano Lett. 13 3594
[34] Braun O M and Kivshar Y S 1998 Phys. Rep. 306 1
[35] Rabe K M 2002 Phys. Today 55 61
[36] Jorio A and Cancado L G 2013 Solid State Commun. 175 3